BBA - Biomembranes 1861 (2019) 495–503

Contents lists available at ScienceDirect

BBA - Biomembranes

journal homepage: www.elsevier.com/locate/bbamem

Different roles for aspartates and glutamates for cation permeation in bacterial sodium channels

Carlo Guardiani[a,b,1], Olena A. Fedorenko[c,d,1], Igor A. Khovanov[a,e], Stephen K. Roberts[c,*]

[a] School of Engineering, University of Warwick, Coventry CV4 7AL, United Kingdom
[b] Department of Physics, University of Lancaster, Lancaster LA1 4YB, United Kingdom
[c] Division of Biomedical and Life Sciences, Lancaster University, Lancaster, United Kingdom
[d] School of Life Sciences, University of Nottingham, Nottingham NG7 2UH, United Kingdom
[e] Centre for Scientific Computing, University of Warwick, Coventry CV4 7AL, United Kingdom

ARTICLE INFO

Keywords:
Voltage-gated sodium and calcium channels
Ion channel selectivity
Molecular Dynamics
Whole-cell patch clamp

ABSTRACT

A key driving force for ion channel selectivity is represented by the negative charge of the Selectivity Filter carried by aspartate (D) and glutamate (E) residues. However, the structural effects and specific properties of D and E residues have not been extensively studied. In order to investigate this issue we studied the mutants of NaChBac channel with all possible combinations of D and E in the charged rings in position 191 and 192. Electrophysiological measurements showed significant Ca^{2+} currents only when position 191 was occupied by E. Equilibrium Molecular Dynamics simulations revealed the existence of two binding sites, corresponding to the charged rings and another one, more internal, at the level of L190. The simulations showed that the ion in the innermost site can interact with the residue in position 191 only when this is glutamate. Based on the MD simulations, we suggest that a D in position 191 leads to a high affinity Ca^{2+} block site resulting from a significant drop in the free energy of binding for an ion moving between the binding sites; in contrast, the free energy change is more gradual when an E residue occupies position 191, resulting in Ca^{2+} permeability. This scenario is consistent with the model of ion channel selectivity through stepwise changes in binding affinity proposed by Dang and McCleskey. Our study also highlights the importance of the structure of the selectivity filter which should contribute to the development of more detailed physical models for ion channel selectivity.

1. Introduction

Voltage-gated sodium and calcium channels (NaV and CaV channels, respectively) are important mediators of many physiological functions, including propagation of electrical signal, cell excitability, gene transcription, secretion and synaptic transmission, plasticity and muscle contraction [1,2]. However, understanding of their structure-function relationships, in particular their ability to select between ions of different size and/or charge, are still poorly understood and remain a major task in membrane biophysics. This problem has attracted much interest within the ion channel community because the high selectivity for a given ion type is associated with high affinity binding (and thus implies a slow release rate), which is at odds with experimental flux rates of up to 10^7 ions/s through individual channels [3]. This counter-intuitive behaviour has been termed the *ion channel paradox*.

Much is now known about cation selectivity and conduction by potassium channels [3-5]. In contrast, computational and experimental studies on bacterial voltage-gated sodium channels (which represent models for understanding selectivity in eukaryotic voltage-gated Na^+ and Ca^{2+} channels) are only beginning to provide insight into cation selectivity and conduction. Analysis of their recently discovered crystal structures identified glutamates in the SF, which form a high field strength (HFS) binding site favouring Na^+ binding with respect to K^+ [6]. Computational studies predict that preferential binding of Na^+ over K^+ is primarily due to the inability of a K^+ ion to bind at the HFS while keeping its hydration shell in the optimal geometric arrangement [7,8]. Our understanding of Na^+/Ca^{2+} selectivity is less well developed. It is well-established that eukaryotic voltage gated Na^+ and Ca^{2+} channels share a similar overall structure at the selectivity filter, albeit with highly conserved "signature" amino acid motifs for Na^+ (DEKA) and Ca^{2+} (EEEE) selective channels. Consequently, it is generally accepted that these channels adopt similar molecular mechanisms for selecting for their preferred cation and selectivity between Na^+ and Ca^{2+} is likely to result from subtle structural differences in the SFs

* Corresponding author.
E-mail addresses: c.guardiani@lancaster.ac.uk (C. Guardiani), s.k.roberts@lancaster.ac.uk (S.K. Roberts).
[1] Equally contributed to this work.

https://doi.org/10.1016/j.bbamem.2018.11.011
Received 19 September 2018; Received in revised form 16 November 2018; Accepted 30 November 2018
Available online 06 December 2018

related to their "signature motifs" [36]. A number of computational studies, using simple physical models have provided a reference theoretical framework to understand selection between Na^+ and Ca^{2+} [8,9]. However validation of these models using experimental measurements and atomistic level simulations is currently missing.

In the present study we used NaChBac, a bacterial voltage-gated sodium channel from *Bacillus halodurans* [10], as a model for structure-function studies of more complex eukaryotic Na^+ and Ca^{2+} voltage-gated channels. NaChBac forms as a homotetramer with each monomer possessing a SF defined by amino acid residues ^{190}LESWAS^{195}. However, despite possessing the Ca^{2+} channel signature EEEE motif in its SF (formed from a ring of four E191 residues), NaChBac selectively conducts Na^+ [10,11]. Indeed, owing to its resemblance to Ca^{2+} channels, it has been suggested to be an ancestor of the eukaryotic counterparts [12]. Functional studies using wild-type and mutated NaChBac (and other bacterial Na^+ channels) have identified the residues which are important for ion selectivity [10,11,13-15]. Most notably, mutations that lead to an increase of negative charge in the SF are sufficient to confer Ca^{2+} selectivity [11]. However, there is no detailed mechanistic explanation for this, despite confirming the importance of charge in the SF (Q_f) in ion permeation and selectivity [9,16]. In an attempt to explain how increasing Q_f leads to Ca^{2+} permeation, we performed whole-cell patch clamp measurements on a series of NaChBac mutants with $Q_f = -8$ (increased from -4 in the wild type NaChBac) differing from each other only in the acidic residue (D or E) in positions 191 and 192. Electrophysiological measurements revealed that the mutants could carry a Ca^{2+} current only when position 191 was occupied by E, while they were impermeable to Ca^{2+} when position 191 was occupied by D. Differences in Ca^{2+} permeation in Cav channels were also reported for substitution of E by D in eukaryotic T-type Ca^{2+} channels [37-39]. In order to provide molecular level understanding of the differential selectivity of the mutants, we performed equilibrium Molecular Dynamics (MD) simulations. The simulations revealed the existence of two ion binding sites (referred to as the extracellular and the intracellular sites). Importantly, the intracellular site was only stabilized through interactions with residue 191 when this was represented by E. Consequently, when E191 is replaced with a D, pronounced differences in the free energy of ion binding at the intracellular and extracellular sites are predicted. We hypothesise that Ca^{2+} permeation (and to a lesser extent also Na^+ permeation) is favoured by a smooth transition from the extracellular to the intracellular SF binding sites and that large differences in the free energy of binding between the two sites results in the ion being trapped at the extracellular site via more stable binding.

2. Methods

2.1. Generation and expression of mutant NaChBac channels

The NaChBac (GenBank accession number BAB05220) cDNA construct containing 274 amino acid residues was synthesised by EPOCH Life Science (www.epochlifescience.com) and subcloned downstream of the CMV promoter (EcoRI/EcoRV) into the mammalian cell expression vector pTracer-CMV2 (Invitrogen). Single amino acid mutations in the pore region of NaChBac were generated by site-directed mutagenesis using oligonucleotides containing the sequence for the desired amino acid substitutions (listed in Supplementary Table 1) and Q5® Site-Directed Mutagenesis Kit (New England BioLabs Inc.). All mutated DNA was sequenced before use. Mutant cDNAs were transiently transfected into CHO cells with TransIT-2020 (Mirus Bio). Transfected cells were identified by GFP fluorescence using an inverted fluorescence microscope (Nikon TE2000-s) and used for electrophysiological investigation 24-48 hours after transfection.

2.2. Electrophysiology

Whole-cell voltage clamp recordings were performed at room temperature (20 °C) using an Axopatch 200A (Molecular Devices, Inc.) amplifier. Patch-clamp pipettes were pulled from borosilicate glass (Kimax, Kimble Company, USA) to resistances between 2 and 3 MOhm. Pipette solution was either PS1 (in mM; 120 Cs-methanesulfonate, 20 Na-gluconate, 5 CsCl, 10 EGTA, and 20 HEPES, pH 7.4 adjusted with 1.8 mM CsOH) or Cs-free PS2 (in mM; 15 Na-gluconate, 5 NaCl, 90 NMDG, 10 EGTA, and 20 HEPES, pH 7.4 adjusted with 3 mM HCl). Standard bath solution was SBS-Na (in mM: 140 Na-methanesulfonate, 5 CsCl, 10 HEPES and 10 glucose, pH 7.4 adjusted with 4.8 mM CsOH) or Cs-free SBS-Na, SBS-Na_x (in mM: 132 Na-methanesulfonate, 5 NaCl, 10 HEPES and 10 glucose, pH 7.4 adjusted with 3.6 mM NaOH). Note that TLDDWAS and TLDEWAS mutants were permeable to Cs^+ (Supplementary Fig. 1), thus Cs-free solutions were used to establish pseudo-bionic conditions. Na^+/Ca^{2+} permeability ratios were determined by replacing 140 mM Na-methanesulfonate in the bath solution with 100 mM Ca-methanesulfonate (SBS-Ca or SBS-Ca_x).

In experiments with varied extracellular Na^+/Ca^{2+} mixtures, GOhm seals were obtained in SBS-Na (or SBS-Na_x for experiments with TLDDWAS and TLDEWAS) containing 10 nM $[Ca^{2+}]_{free}$, followed by replacement of the bath solution according to Supplementary Table 2 to vary the Ca^{2+} activity. $[Ca^{2+}]_{free}$ were calculated using Webmaxc (http://web.stanford.edu/cpatton/webmaxcs.htm). Na^+ and Ca^{2+} (for 10 mM, 50 mM and 100 mM) activities were calculated using the Debye-Huckel equation (we consider $[Ca^{2+}]_{free}$ = ion activity of Ca^{2+}); for details see Supplementary Table 2.

Osmolarities of all solutions were measured using a Wescor vapor pressure osmometer (model 5520) and adjusted to 280 mOsm kg^{-1} using sorbitol. All solutions were filtered with a 0.22-mm filter before use. Whole cell currents were recorded 3 min after obtaining whole cell configuration to ensure complete equilibration of the pipette solution and cytosol. The bath solution was grounded using a 3 M KCl agar bridge; the liquid junction potential, determined experimentally as described by Neher [32], was negligible and was not accounted for. The recording chamber volume was approximately 200 µ l and was continuously exchanged by a gravity-driven flow/suction arrangement at rate of ~2 ml/min; to ensure complete exchange of bath solution. Electrophysiological recordings were initiated after > 4 min of continuous solution change.

Results were analysed using Clampfit 10.1 software (Molecular Devices) and Origin9.1 (OriginLab). Data are presented as means ± SEM(n), where n is the number of independent experiments.

2.3. Molecular Dynamics simulations

We used as a starting structure to build NaChBac mutants TLEDWAS, TLDEWAS, TLDDWAS and TLEEWAS the homology model of wild-type NaChBac (TLESWAS) that we built using as a template the structure of the NavMs channel featuring 45% sequence identity (PDB ID: 4F4L). The details of the homology model building are provided in Ref [17]. Mutations and embedding in a membrane of 248 POPC molecules was performed using the CHARMM membrane builder [19,20]. The membrane was bathed on both sides by a 140 mM NaCl solution or a 100 mM $CaCl_2$ solution. All simulations were performed with the NAMD [21] suite of programs using the ff14SB [22] force field for the protein and the Lipid14 force-field [23] for the phospholipids. As already observed in Ref [24], in the absence of harmonic restraints the pore rapidly closes at the cytoplasmic gate. In order to avoid this behaviour that likely results from the absence of the Voltage Sensor Domain in the simulated system, harmonic restraints (50 kcal/mol/Å^2) were applied to the backbone atoms of the transmembrane helices (residues 151–175 and 218–247) throughout the simulation. The eight systems first underwent 10,000 steps of conjugate gradient minimization. During equilibration harmonic restraints were applied to non-

hydrogen atoms of the protein backbone and side-chains (outside the transmembrane helices; residues 176–217) as well as to the phospholipid heads. An harmonic restraint was also applied to the dihedral angle formed by Carbons 8, 9, 10, 11 of oleoyl acid and to the improper dihedral $C_1 - C_3 - C_2 - O_2$ involving the three carbons of the glycerol unit and the hydroxyl oxygen linked to its central carbon. The equilibration was organized in six stages whereby the constraints were gradually released. The values of the force constants used in the six stages can be found in Supplementary Table 3. The production run was carried out in the isothermal isobaric (NPT) ensemble for 100 ns. Pressure was kept at 1 atm by the Nose-Hoover Langevin piston method while temperature was kept at 300 K by coupling to a Langevin thermostat with damping coefficient of $1\ ps^{-1}$. Long-range electrostatic interactions were evaluated with the smooth particle mesh Ewald algorithm. For the short-range non-bonded interactions, we used a cutoff of 12 Å with a switching function at 10.0 Å. The integration time step was 2 fs, and the bonds between hydrogen and heavy atoms were fixed to eliminate the most rapid oscillatory motions. The Potential of Mean Force (PMF) was computed using an expression proposed by Roux and coworkers [40]: $\Delta G(z) = -k_B T \log\left(\frac{\rho(z)}{\rho_{bulk}}\right)$ where k_B is Boltzmann constant, T is the absolute temperature, $\rho(z)$ is ion density at axial level z and ρ_{bulk} is ion density in the bulk phase. The convergence of the PMF profiles shown in Fig. 5 and in Supporting Fig. 9 was assessed by repeating the calculation in increasingly long blocks of the trajectory (0–20 ns, 0–40 ns, 0–60 ns, 0–80 ns and 0–100 ns). As illustrated in Supporting Figs. 10 and 11 the PMF profiles computed at different times are very similar and as the simulation proceeds the curves become closer and closer to one another. Indeed after 40 ns, the PMF profiles practically collapse onto one another signalling the onset of a converged state.

3. Results

3.1. Experimental results

3.1.1. Na^+ and Ca^{2+} Selectivity of Mutated NaChBac Channels

The SF in NaChBac is defined by the seven amino acid motif of ^{189}TLESWAS^{195}. Using site-directed mutagenesis we generated mutant channels with different combinations of E and D at positions 191 and 192. NaChBac channels were heterologously expressed in CHO cells and whole cell currents were recorded using the patch-clamp technique (Fig. 1). Permeability ratios (P_{Ca}/P_{Na}) were determined from changes in whole cell current reversal potentials (E_{rev}) following complete exchange of extracellular 140 mM Na^+ with 100 mM Ca^{2+} (Table 1).

In standard bath solution (in which Ca^{2+} was not buffered), the magnitude of peak inward current exhibited by TLEDWAS, TLEEWAS and TLDEWAS channels were stable over time (tested by repetitive depolarisations to −10 mV every 20 s; Supplementary Fig. 2). In contrast, the magnitude of peak inward current exhibited by TLDDWAS channels decreased significantly with time (Supplementary Fig. 2). Interestingly, the decrease in TLDDWAS-mediated currents was only observed at test potentials eliciting inward current (−10 mV) and not at test potentials eliciting outward currents (+70 mV; Supplementary Fig. 2b). Furthermore, addition of 10 mM EGTA to the bath solution also prevented current decrease (Supplementary Fig. 2b). Taken together, these results are consistent with high affinity voltage dependent Ca^{2+} blockade of TLDDWAS channels in which contaminant levels of Ca^{2+} in unbuffered SBS-Na solution was sufficient to inhibit Na^+ permeation through TLDDWAS channels. A similar Ca^{2+} dependent block of TLDDWAS equivalent mutant has been reported in the NavAb bacterial sodium channel [15]. Therefore, recordings of Na^+ influx from cells expressing TLDDWAS were conducted using SBS-Na_x supplemented with 10 mM EGTA (Fig. 1).

Table 1
The whole cell peak current densities obtained for channel mutants in 140 mM extracellular Na^+ or in 100 mM extracellular Ca^{2+}. P_{Ca}/P_{Na} ratios were calculated from E_{rev} values determined from current-voltage relationships shown in Fig. 2.

SF	I_{peak} Na (pA/pF)	I_{peak} Ca (pA/pF)	P_{Ca}/P_{Na}
TLEEWAS	13.6 ± 2.9 (n = 16)	8.1 ± 1.8 (n = 9)	15.4 ± 0.6 (n = 9)
TLEDWAS	55.2 ± 8.6 (n = 14)	25.9 ± 8.1 (n = 11)	43.2 ± 4.1 (n = 11)
TLDEWAS	13.0 ± 3.6 (n = 10)	No currents (n = 9)	–
TLDDWAS	17.3 ± 3.4 (n = 14)	No currents (n = 16)	–

In agreement with previous publications [11,33] the S192D mutation (generating TLEDWAS) was permeable to both Na^+ and Ca^{2+}. In the presence of 140 mM extracellular Na^+ (SBS-Na), TLEDWAS-mediated whole cell currents were 4-fold greater than that mediated by TLEEWAS, TLDEWAS and TLDDWAS channels (Fig. 1). Replacing extracellular Na^+ with 100 mM Ca^{2+} (SBS-Ca) TLEDWAS-mediated currents (maximal peak current density of 25.9 ± 8.13 pA/pF; n = 11) reversed at 71.5 ± 1.26 mV (n = 11; Fig. 1c), indicating a permeability ratio in favour for Ca^{2+} (P_{Ca}/P_{Na} = 43.2 ± 4.06); though comparison of maximal peak current amplitudes in the presence of Ca^{2+} with those in the presence of Na^+ revealed the I_{Ca}/I_{Na} ratio of 0.34 ± 0.16 (n = 11) indicating favourable Na^+ permeation. TLEEWAS was less permeable to Ca^{2+} (P_{Ca}/P_{Na} = 15.4 ± 0.6 and I_{Ca}/I_{Na} = 0.25 ± 0.02 (n = 9) and no Ca^{2+} inward current was detectable for TLDEWAS and TLDDWAS (Fig. 1).

To study permeability for Na^+ and Ca^{2+} for TLEDWAS, TLEEWAS, TLDEWAS and TLDDWAS in more detail, bath solutions containing Na^+ and Ca^{2+} in varying concentrations were used to investigate divalent blockade. Specifically, maximal current density was determined from

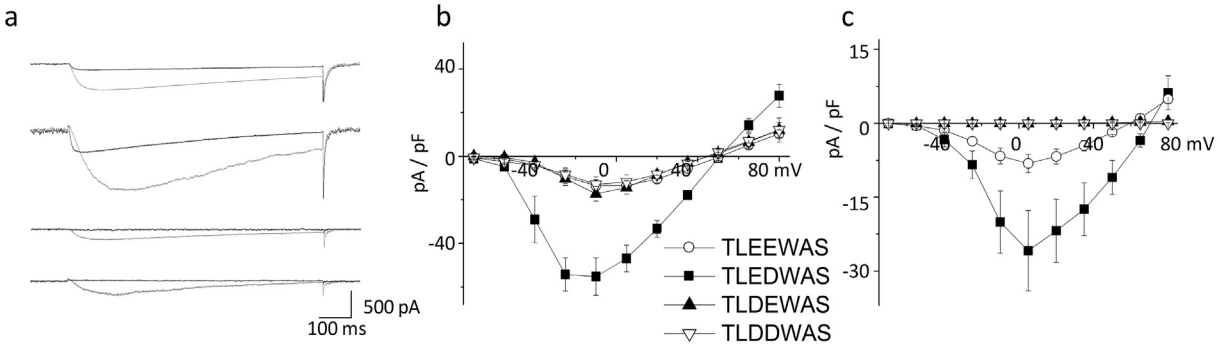

Fig. 1. Na^+/Ca^{2+} selectivity of NaChBac mutant channels. Currents recorded in 140 mM Na^+ (grey traces) or 100 mM Ca^{2+} (black traces) bath solutions for (from top to bottom) TLEEWAS, TLEDWAS, TLDEWAS, and TLDDWAS channels in response to a step to −10 mV from V_{hold} = −100 mV. Mean (± SEM) current-voltage relationships of peak whole-cell currents elicited by series of step depolarizations (starting from +95 mV to −85 mV in −15 mV steps) from V_{hold} of −100 mV in 140 mM Na^+ (b) or in 100 mM Ca^{2+} (c) bath solution. Note that the bath solution containing 140 mM Na^+ was supplemented with 10 mM EGTA for recording of Na^+ currents elicited by TLDDWAS.

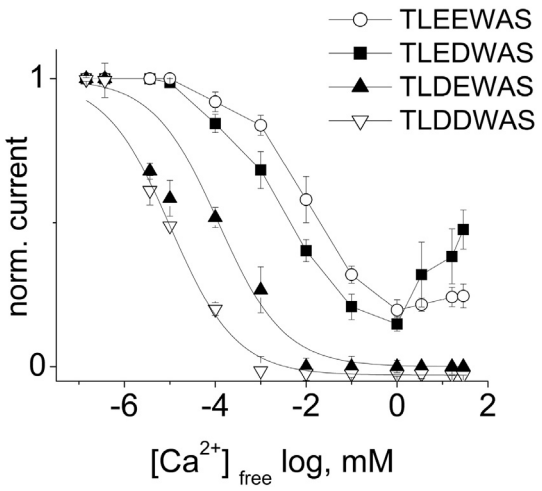

Fig. 2. Ca^{2+} blockade of NaChBac-mediated currents for channels. Mean (± SEM) whole-cell maximal peak NaChBac-mediated currents recorded in standard bath solution (SBS-Na or SBS-Na_x), in which Ca^{2+} was added (up to 100 μM) or Na^+ replaced with equimolar Ca^{2+} (from 1 to 100 mM) (see details in Supplementary Table 2). Data fitted with $y = A1 + (A2 - A1)/(1 + 10^{((\log x0 - x)*p)})$.

I–V relationships using bath solution with increasing Ca^{2+} content (Supporting Table 2 for details of solutions). This permitted the determination of half maximal (IC_{50}) current values which reflect the affinity of Ca^{2+} for binding in the pore of the channel; specifically, 38 μM for TLEEWAS, 6 μM for TLEDWAS, 117 nM for TLDEWAS and 10.4 nM for TLDDWAS (Fig. 2). Note that the high affinity binding of Ca^{2+} in TLDDWAS is consistent with the blockade of this channel by contaminant levels of Ca^{2+} in SBS-Na (supplementary Fig. 2). MD simulations of TLEDWAS, TLEEWAS, TLDEWAS and TLDDWAS were conducted in an attempt to provide a molecular basis for their different Ca^{2+} and Na^+ permeation properties.

3.2. Computational results

MD simulations of the NaChBac mutants were performed using either Ca^{2+} (at 100 mM) or Na^+ (at 140 mM); however, in the interest of clarity and to reflect the focus on Ca^{2+} permeation in NaChBac mutants with $Q_f = -8$, we primarily report the MD simulations results with Ca^{2+}. Our simulations using Na^+ ions are reported in the Supporting Information and only brief reference to Na^+ ion permeation will be made in the following sections.

3.2.1. Selectivity Filter occupation

Important insight into the selectivity of NaChBac mutants with $Q_f = -8$ was attained through 100 ns equilibrium simulations in the NPT ensemble. Fig. 3 shows the time course for the number of Ca^{2+} ions occupying the Selectivity Filter (SF: $2 < z < 14$ Å) when simulated in a 100 mM $CaCl_2$ solution. Notably, the SF is rapidly (within 20 ns) and stably occupied by two Ca^{2+} ions which is in contrast with simulations (in 0.5 M $CaCl_2$) for wild-type ($Q_f = -4$) NaChBac [18], which revealed the SF to be occupied by a single Ca^{2+} ion (with the entry of a second Ca^{2+} ion being electrostatically repelled).

Analysis of the atom and ion arrangements in the SF of the NaChBac $Q_f = -8$ mutants (based on the final frame of the 100 ns runs in 100 mM $CaCl_2$; Supp. Figs. 3 and 4) revealed one Ca^{2+} ion in the upper part (the extracellular ion) and one in the lower part (the intracellular ion) of the SF. Interestingly, the extracellular Ca^{2+} ion was coordinated by multiple D and/or E residue side-chains while the intracellular ion was hydrated by more water molecules and interacted with fewer acidic residues. Significantly, the difference between the two Ca^{2+} ions with respect to their level of interaction with the SF was more pronounced when the residue in position 191 was D (TLDDWAS and TLDEWAS). A detailed description of the Ca^{2+} interactions in the SF of the NaChBac $Q_f = -8$ mutants can be found in the Supporting Information. However, of particular note is that the side chains of D191 residues form H-bonds with the backbone amide groups of W193 and A194 and the side chains of S195, leaving the carboxyl side chains of the D191 tangentially orientated with the wall of the channel pore (and unable to directly interact with the resident Ca^{2+} ions). In contrast, most of the side chains of the E191 residues in TLEEWAS and TLEDWAS remain available to directly co-ordinate the resident Ca^{2+} ions. A consequence of this different arrangement of the side chains at position 191 was that only the extracellular Ca^{2+} ion in TLDEWAS and TLDDWAS directly binds to the SF via residue 192; the intracellular Ca^{2+} ion only indirectly interacts with the residues forming the SF via the 9 water molecules of its hydration shell. In contrast, the carboxyl side chains from both residues 191 and 192 in TLEDWAS and TLEEWAS point towards the centre of the pore in such a way that both residues interact with the extracellular ion while the intracellular ion is co-ordinated by several E191 side chains. A summary of Ca^{2+} co-ordination in the SF of the NaChBac mutant channels is given in Table 2.

Our simulations suggest that the inability to directly co-ordinate the intracellular Ca^{2+} ion in the SF of the D191 mutants might be a crucial factor in determining Ca^{2+} permeability and/or blockade of the NaChBac $Q_f = -8$ mutants. Thus, this phenomenon was characterized in more detail in Fig. 4 which shows the time course plot of the distance between the four residue side chains at position 191 and the intracellular Ca^{2+} ion over a 100 ns simulation. Due to the rotational freedom of the side chains of D and E residues for each frame we show the distance between the calcium ion and the closest ϵ-oxygen of E191 or δ-oxygen of D191. The distance cutoff for Ca^{2+}-oxygen interaction was set to $d_c = 3.5$ Å which corresponds to the position of the first minimum of the Radial Density Function (RDF) of the distance between calcium and the oxygen of bulk water [18]. Fig. 4 confirms that for the D191 mutant channels, the δ-oxygen was too far away to directly bind to the intracellular Ca^{2+} ion over the 100 ns period (reflecting its tangential orientation with the axis of the pore). In contrast, in the E191 mutant channels, at least one of the ϵ-oxygens is constantly close enough to the intracellular ion to enable Ca^{2+}-oxygen interaction and in the case of TLEDWAS, three of the side chain oxygens are close enough over most of the 100 ns period.

We surmised that D191 mutant channels do not permit Ca^{2+} permeation (Fig. 1 C and D) because of a large difference in binding free energies associated with the two resident Ca^{2+} ions; specifically, the extracellular ion (which is chelated by residue 191 and/or 192) possessing a higher free energy of binding and the intracellular ion (which is fully hydrated with only indirect interaction with the pore residues) having a much lower free energy of binding. Based on our simulations it can thus be suggested that the direct binding of both resident Ca^{2+} ions in the SF of the E191 mutants resulted in equivalence in the binding energies for the Ca^{2+} ions and thus an energy landscape that was thermodynamically favourable for ion permeation.

3.2.2. Potential of mean force

Fig. 5 shows the PMF of Ca^{2+} derived from the NPT simulations in 100 mM $CaCl_2$. For all the mutants the PMF is characterized by the presence of two main minima that mark the positions of the binding sites of the two Ca^{2+} ions occupying the SF. The minimum at $z = 5$–6 Å (S1) identifies the binding site for the intracellular ion (at the level of L190) while the minimum at $z = 10$–11 Å (S2) corresponds to a binding site for the extracellular ion in the upper part of the SF at the level of the glutamate and aspartate ring at positions 191 and 192. Fig. 5 illustrates why the TLDEWAS and TLDDWAS mutants have a limited (if any) calcium permeability. First, the transition barrier between S2 and S1 is greater than 7.0 –7.5 kcal/mol suggesting that the transition from S2 to S1 (*i.e.* Ca^{2+} influx) in D191 mutants would be kinetically forbidden. Second, the minimum S1 is 1.0 –1.5 kcal/mol higher in free

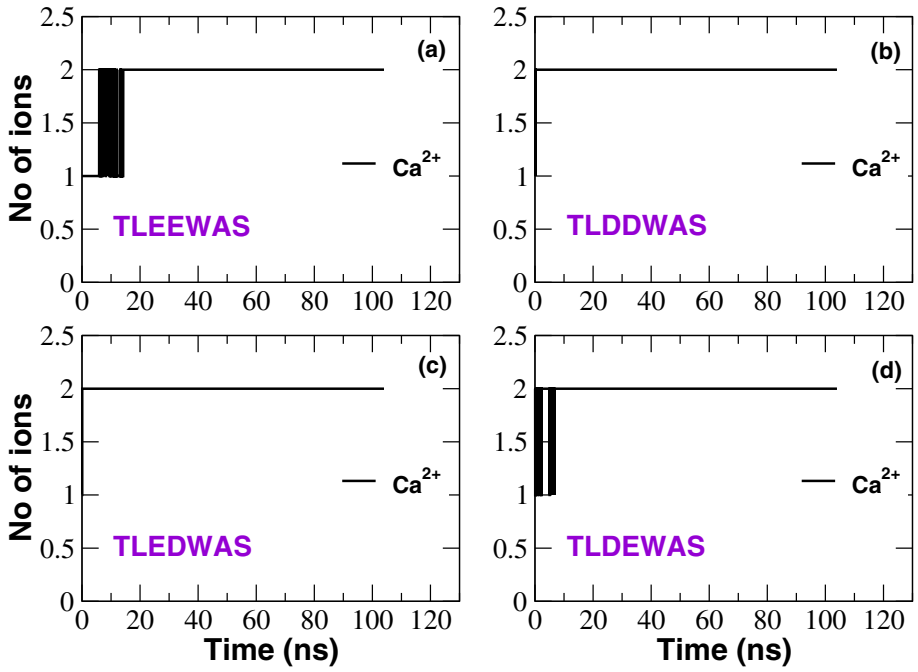

Fig. 3. Time course of the number of calcium ions (black line) occupying the SF of TLEEWAS (a), TLDDWAS (b), TLEDWAS (c) and TLDEWAS (d). Simulations were performed in a 100 mM $CaCl_2$ solution.

Table 2
Ca^{2+} ion co-ordination and side chain orientation of the aspartate and glutamate residues at positions 191 and 192 in the SF of the NaChBac mutants exhibiting $Q_f = -8$. The last two columns detail the number of water molecules coordinated (wat) and the number of aspartate and glutamate residues of the two charged rings coordinating the two resident ions.

Mutant	Residue position 191	Residue position 192	Ca^{2+}_{intra}	Ca^{2+}_{extra}
TLDDWAS	D: All four side chains are tangentially oriented along the axis of the pore	D: Two side chains coordinated with the extracellular Ca^{2+} ion	D191: 0	D191: 0
			D192: 0	D192: 2
			wat: 9	wat: 4
TLDEWAS	D: All four side chains are tangentially oriented along the axis of the pore	E: All four side chains coordinated with the extracellular Ca^{2+} ion	D191: 0	D191: 0
			E192: 0	E192: 4
			wat: 9	wat: 4
TLEDWAS	E: One side chain tangentially oriented along the axis of the pore, three side chains each coordinated with both resident Ca^{2+} ions simultaneously	D: Two side chains coordinated with resident extracellular Ca^{2+} ion	E191: 3	E191: 3
			D192: 0	D192: 2
			wat: 6	wat: 3
TLEEWAS	E: Two side chains tangentially oriented along the axis of the pore, two side chains each coordinated with both resident Ca^{2+} ions simultaneously	E: Three side chains coordinated with resident extracellular Ca^{2+} ions.	E191: 2	E191: 2
			E192: 0	E192: 3
			wat: 5	wat: 2

energy with respect to that at S2. Note that the PMF depends logarithmically on the relative ion density, $F(z) = -k_B T \log(\rho(z)/\rho_{bulk})$, so that a free energy difference of 1.0 –1.5 kcal/mol between the two binding sites means that the relative density of calcium in the extracellular site is approximately 3–5 times higher than at the intracellular site. This difference in Ca^{2+} density is partly due to a narrowing of the extracellular side of the SF (where the D and E side chains are projected towards the centre of the channel) and partly due to the greater stability of the extracellular binding site (because the calcium ion is coordinated by several acidic residues). The movement of a Ca^{2+} ion between the binding sites is thus predicted to be thermodynamically unfavourable.

When position 191 is occupied by E, the free energy landscape is more favourable for Ca^{2+} permeation. Fig. 5 shows that the two main minima corresponding to the binding sites S1 and S2 are broader and split into several sub-basins (with the barriers between the binding sites being relatively shallow). In TLEEWAS the difference between S1 and S2 is 0.5 kcal/mol and note that the transition barriers between S1 and S2 are also relatively small (2.0 –3.0 kcal/mol) and can be easily overcome. The scenario is even more favourable for Ca^{2+} permeation in TLEDWAS where the transition barrier is also relatively small at approximately 3.5 kcal/mol, and the two minima are isoenergetic; this probably reflects the fact that the E191 residue is able to co-ordinate the intracellular Ca^{2+} ion making it comparable to the extracellular Ca^{2+}.

3.2.3. Ion hydration and coordination

The PMF profiles mainly reflect the balance between the desolvation cost of the ions and the gain in electrostatic potential energy due to the interaction with the fixed charges of the SF. In order to understand the PMF profiles with respect to Ca^{2+} permeation through the NaChBac mutants, we plot the average number of oxygen atoms interacting with Ca^{2+} ions in transversal bins with a height of 2.0 Å. In particular the analysis will be focused on the coordination pattern of the Ca^{2+} ions in binding sites S1 and S2 (Fig. 5). Fig. 6 and Table 3 show that when the

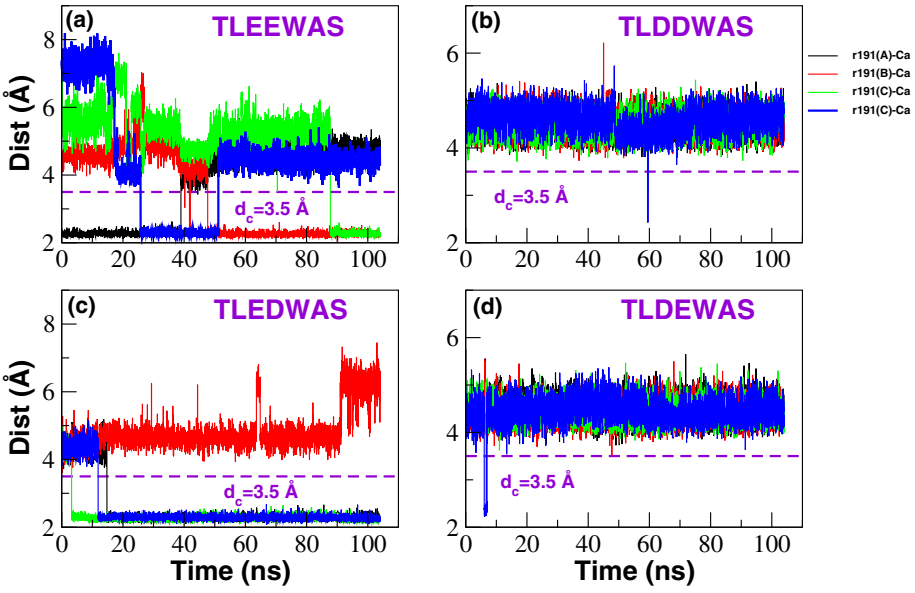

Fig. 4. Coordination of the lower Ca^{2+} ion resident in the SF of NaChBac mutants during simulations in 100 mM $CaCl_2$. The curves show the distance between this calcium ion and the closest ϵ oxygen of E191 (a, c) or the closest δ oxygen of D191 (b, d). The dashed lines represents the cutoff distance below which the calcium ion becomes coordinated by the side chain of acidic residues. Panels (a), (b), (c) and (d) correspond to mutants TLEEWAS, TLDDWAS, TLEDWAS and TLDEWAS respectively.

Ca^{2+} ion moves from site S2 to S1, the ion undergoes a net loss of coordinating negatively charged oxygens provided by the acidic side chains of the acidic residues at positions 191 and 192 (n_{DE}) and an increase in the number of the coordinating water molecules (n_w). In particular, as detailed in Table 3, the number of gained water molecules (Δn_w) is approximately equal to the number of lost acidic oxygens (Δn_{DE}) so that $\Delta n_w \sim \Delta n_{DE}$. If ΔG_{DE} and ΔG_w indicate the free energy of interaction of a Ca^{2+} ion with a single acidic oxygen and a single water molecule respectively, then the total free energy change the calcium ion experiences while moving from site S2 to site S1 can be expressed as:

$$\begin{aligned}\Delta G_{tot} &\cong \Delta n_{DE}\Delta G_{DE} + \Delta n_w \Delta G_w \\ &\cong \Delta n_{DE}\Delta G_{DE} - \Delta n_{DE}\Delta G_w \\ &= \Delta n_{DE}(\Delta G_{DE} - \Delta G_w)\end{aligned} \quad (1)$$

As the term $\Delta G_{DE} - \Delta G_w$ can be considered as a constant, the above approximation enables us to express the free energy change of a Ca^{2+} ion moving from S2 to S1 as a function of Δn_{DE} only; *viz*, TLEDWAS $\Delta n_{DE} = -1.3$; TLDEWAS $\Delta n_{DE} = -6.53$; TLDDWAS $\Delta n_{DE} = -3.77$; TLEEWAS $\Delta n_{DE} = -2.0$. The movement of Ca^{2+} from the extracellular to the intracellular binding site (i.e. Ca^{2+} influx) thus demands the lowest thermodynamic cost in TLEDWAS and in TLEEWAS in agreement with the experimental recordings of Ca^{2+} currents in these mutants (Fig. 1).

This modest cost is due to the ability of E191 to coordinate the Ca^{2+} at S1, thus partially compensating the loss of the coordinating acidic side chains from residue 192 as the Ca^{2+} ion moves from S2 to S1. The fact that this compensation is not possible when position 191 is occupied by an aspartate residue explains the high thermodynamic penalty incurred by the Ca^{2+} ion when travelling from S2 to S1 in TLDEWAS and TLDDWAS. Note that a similar analysis can be applied to the transition of the Na^+ ion from site S2 to site S1 expressing the free energy change as a function of Δn_{DE} only. As detailed in the Supporting Information (and illustrated in Supporting Fig. 9 and Supporting Table 4), the calculation reveals that Na^+ undergoes the minimal loss of

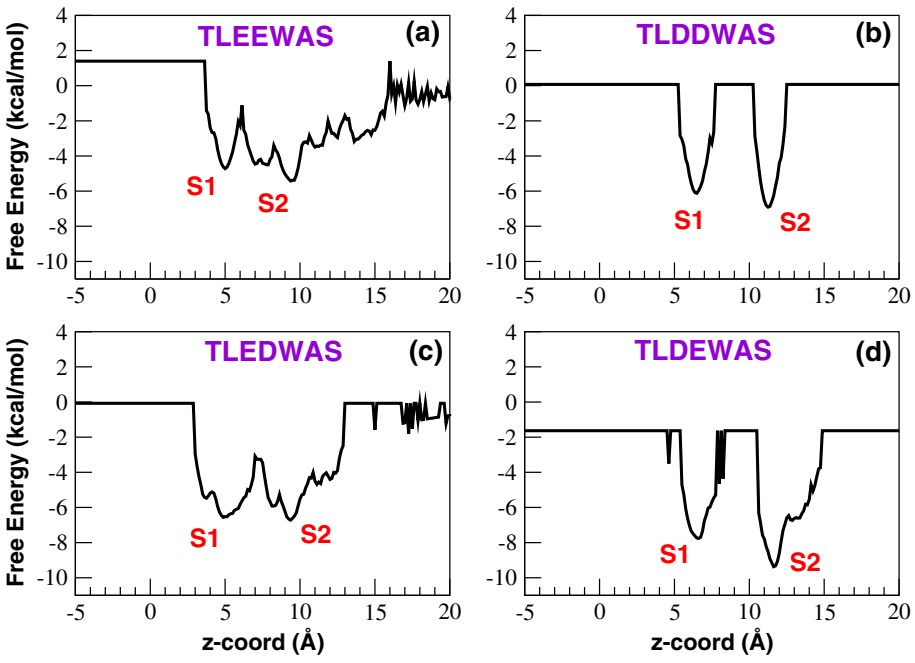

Fig. 5. Potential of Mean Force of calcium ion in mutants TLEEWAS (a), TLDDWAS (b), TLEDWAS (c) and TLDEWAS (d) as a function of the axial position in the SF. The PMFs have been computed from 100 ns unbiased simulations in the NPT ensemble. The system was bathed by a 100 mM $CaCl_2$ solution. The intracellular and extracellular binding sites are labelled S1 and S2 respectively.

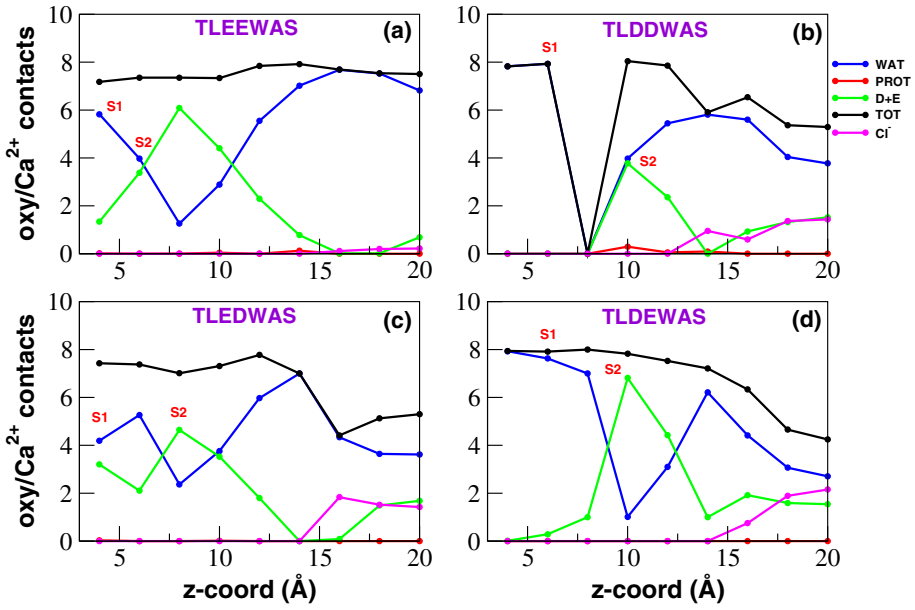

Fig. 6. Calcium hydration and coordination in NaChBac mutants TLEEWAS (a), TLDDWAS (b), TLEDWAS (c) and TLDEWAS (d) in equilibrium simulations in a 100 mM $CaCl_2$ solution. Number of coordinating oxygens and chlorides in axial bins with a height of 2.0 Å computed using a cutoff distance of 3.5 Å for both Ca^{2+}-oxygen and Ca^{2+}-Cl^-. Blue line: number of coordinating oxygens provided by water; green line: coordinating oxygens contributed by glutamates and/or aspartates; red line: oxygens contributed by other protein residues; black line: total number of coordinating oxygens; magenta line: number of coordinating chlorides. The labels S1 and S2 mark the position of the binding sites corresponding to the two main minima of the PMFs in Fig. 5 and Supporting Fig. 7.

Table 3
Accountancy of calcium-coordinating waters (n_w) and acidic oxigens (n_{DE}) in the intracellular (S1) and extracellular (S2) binding sites in the SF of NaChBac mutants. Simulations were performed in a 100 mM $CaCl_2$ solution.

Site	n_{oxy}	TLEDWAS	TLEEWAS	TLDEWAS	TLDDWAS
S1	n_{DE}	3.2	1.3	0.27	0.0
S1	n_w	4.2	5.8	7.60	7.93
S2	n_{DE}	4.5	3.3	6.8	3.77
S2	n_w	2.5	4.0	1.0	3.97
S1–S2	Δn_{DE}	−1.3	−2.0	−6.53	−3.77
S1–S2	Δn_w	+1.7	+1.8	+6.6	+3.96

acidic coordinating oxygens in TLEDWAS in agreement with the higher sodium currents experimentally recorded for this mutant.

4. Discussion and conclusions

The different roles of D and E residues in the SF of ion channels have not been studied extensively. A remarkable exception is represented by studies from Nilius lab [37-39] on T-type Ca^{2+} channels. T-type channels are characterized by a EEDD ring in the SF which differs from the EEEE locus found in high voltage activated channels. Talavera et al. showed [37-39] that a single D to E mutation in the EEDD locus could be sufficient to alter the Ca^{2+}/Ba^{2+} selectivity, the anomalous mole fraction effect between Ca^{2+} and Ba^{2+}, the Cd^{2+} sensitivity and proton block. In order to extend the characterization of the differential roles of acidic D/E residues in the SF in this work the effect of the structure of the SF was investigated through the analysis of NaChBac mutants with all possible combinations of D and E in positions 191 and 192 (TL**ED**WAS, TL**DE**WAS, TL**DD**WAS and TL**EE**WAS). Despite having the same SF charge $Q_f = -8$ the four mutants exhibit different electrophysiological behaviour with respect to Ca^{2+} permeation. In particular, E191 results in Ca^{2+} permeability, while D191 results in high affinity Ca^{2+} block. Molecular dynamics simulations in NaCl and $CaCl_2$ solution revealed the existence of two binding sites. The ion in the extracellular higher affinity binding site is coordinated by multiple D and/or E side chains while the intracellular resident cation interacts with fewer (or no) acidic side chains and is coordinated by more water molecules. Based on these findings we formulate an hypothesis to rationalize the different electrophysiological behaviour of the mutants. When position 191 is occupied by D, an ion moving from the extracellular to the intracellular binding site experiences a significant decrease of the free energy of binding which is expected to impede Ca^{2+} permeation; the same transition is smoother when position 191 is occupied by E and is consistent with Ca^{2+} permeation. It is worth noting that ion permeation requires not only small barriers between the two binding sites but there must be a low barrier also between the innermost site and the central cavity. In our simulations however, this barrier is artificially high since the PMF depends on the local ion density and in our simulations in the absence of an external electric field, no transition from the SF to the Central Cavity could be observed.

Recently Tang et al. [15] have introduced analogous mutations in the NavAb channel and have performed a detailed crystallographic analysis of the mutants. The SF sequence in NavAb is ^{175}TLESWSM^{181} so that ^{175}TLDDWSM^{181} is equivalent to NaChBac mutant TLDDWAS. Three Ca^{2+} binding sites were identified in TLDDWSM (labelled 1 to 3 from the extracellular to the intracellular side). In Site-1 the calcium ion mainly interacts with the side chains of D178, in Site-2 it interacts with the carboxylates of D177 and the backbone carbonyls of L176 and in Site-3 it binds the backbone carbonyls of T175. Due to high electrostatic repulsion, it is unlikely that the three sites can be simultaneously occupied and the crystal structures are likely to arise from the superposition of two families of conformations with occupation of sites 1, 3 and 2 respectively. Thus, structures of NavAb mutants are in line with our equilibrium simulations which show multiple occupancy in the selectivity filter. It is also striking that the side-chains of D177 in TLDDWSM are aligned along the walls of the SF rather than projecting into the lumen, thus mirroring the predicted behaviour of the D191 residues in the NaChBac mutants. Also in agreement with the present study, the NavAb TLEDWSD mutant (equivalent to the TLEDWAS NaChBac mutant) structure showed the carboxyl group of E177 swing away from the channel lumen to establish H-bonds with the backbone amide groups of other residues of the same chain.

This picture emerging from our simulations also fits well within the conceptual framework of ion channel selectivity through stepwise changes in binding affinity proposed by Dang and McCleskey [25]. Many selectivity models have been proposed to solve the *conductivity/selectivity paradox* of ion channels. In fact, the high selectivity of ion channels was traditionally explained in terms of a single high-affinity binding site for the selected ion. However, this would imply high exit barriers and slow release of ions at odds with experimentally measured permeation rates close to the free diffusion limit. In order to solve this paradox, permeability for Ca^{2+} is often described in terms of high

affinity neighbouring binding sites (with lower affinity for competing cations) with electrostatic repulsion between ions when the two sites are simultaneously occupied; this lowers the barrier to cation exit from the pore resulting in permeation. However, in the "step model" by Dang and McCleskey, ion repulsion is not necessary for permeation, rather the potential energy profile (characterized by a deep central well flanked by shallower low affinity minima) is such that the high potential energy barrier associated with the lowest minimum is split into two smaller barriers enabling the permeating ion to overcome smaller barriers in successive steps. Once the ion has reached the intermediate step, it can face the next barrier with no memory of the energy expended in reaching there due to fast thermal re-equilibration. It is noteworthy that repulsive interactions between ions are not required by the model to explain permeation, but multiple occupancy of neighbouring binding sites is nevertheless not excluded and the occurrence of this event is predicted to enhance Ca^{2+} flux. The step model thus represents an alternative and original mechanism to explain the conductivity/selectivity paradox. Recently, the step model has been validated and shown to describe experimentally recorded currents from a T-type calcium channel [26,27] and predicts a high affinity external site and an internal lower affinity Ca^{2+} binding site similar to that shown in our MD simulations of NaChBac mutants. This shows that not only 3-site models like Deng and McCleskey's but also 2-site models can capture the behaviour of Ca^{2+} channels. Furthermore, the step model provides a useful framework to understand the ranking of Ca^{2+} permeability experimentally determined for the NaChBac mutants; *viz.*, the NaChBac mutant exhibiting greatest calcium permeability is TLEDWAS and this mutant exhibits a PMF profile with near isoenergetic minima.

Normally the minima of an energy profile are interpreted as binding sites *i.e.* protein districts with an arrangement of side chains creating an environment sterically and chemically complementary to the ligand. However, Dang and McCleskey suggest that the low affinity minimum is better considered as any mechanism capable of changing the potential energy of the permeating ion (*e.g.* as a result of partial rehydration of the ion). The MD simulations of D191 mutants are an example of this principle. Although the side chains of residue D191 point away from the innermost permeating ion (and thus not forming a binding site according to the classical biochemical definition), our simulations show that the ion sitting in the intracellular site is coordinated by more water molecules acting as bridges with the protein. This generalization of the concept of binding site provides a powerful conceptual framework capable of reconciling conflicting views on the electrophysiology of ion channels. For example, in fact, most biophysical models postulate the existence of at least two Ca^{2+} binding sites; yet early functional studies [34,35] on vertebrate calcium channels identified only a single high affinity binding site (*viz.* replacement of all the four E residues of the SF with glutamines or alanines was sufficient to abolish Ca^{2+} block of monovalent ions current consistent with the four E residues forming the only Ca^{2+} binding site). These conflicting data could be reconciled assuming the existence of a single classical high affinity binding site (where Ca^{2+} binding causes the block of monovalent cation current) and a generalized binding site (according to the definition of Dang and McCleskey) necessary to promote high conductance ion permeation.

Thus, we feel that our hypothesised explanation for the differing Ca^{2+} permeation characteristics of the NaChBac mutant channels is robust and worthy of further validation; *viz.*

- Extending the MD simulations to Free Energy Perturbation calculations which could be used to calculate the free energy of binding of ions at the two identified binding sites in the SF.
- Extending the experimental validation by preventing D191 side chain from establishing H-bonding with the backbone amide groups of W193 and A194 and the side chain of S195. It is predicted that the D191 mutants would show equivalent ion permeation characteristics to that of their E191 counterparts. Specifically, we suggest that site directed mutagenesis could be employed to (*i*) generate S195A mutation and prevent H-bonding to the serine side chain, (*ii*) replace W193 and A194 with prolines so as to disrupt H-bonding with the amide groups in the SF backbone and (*iii*) generate N-methylated variants of W193 and A194 which should also prevent H-bonding to the amide groups [28-30].

In conclusion, our MD simulations offer an explanation for different cation permeability characteristics for voltage gated channels exhibiting the same nominal charge density in the SF but displaying different ion permeation properties. In addition, as discussed in detail in the Supporting Information, the structural arrangement of side chains in the SF shown by our simulations, suggests that the effective charge perceived by an incoming cation might be different from the nominal one in agreement with the predictions of the ionic Coulomb Blockade model [31]. Our work thus, highlights how the structure of the SF can be as important as its charge in determining ion permeability and selectivity and allows the formulation of an hypothesis, in agreement with the step model of Dang and McCleskey, that could shed light on a new mechanism of modulation of ion channel selectivity.

Author contributions

Patch-clamp experiments were performed by Olena Fedorenko (OF), computational simulations by Carlo Guardiani (CG); conception and design of the work by OF, CG, Stephen Roberts (SR) and Igor Khovanov (IK); acquisition, analysis and interpretation of data for the work by OF, SR and CG, drafting the work by OF, SR and CG, revising it critically for important intellectual content by SR, IK and CG. All authors approved the final version of the manuscript. All persons designated as authors qualify for authorship, and all those who qualify for authorship are listed.

Transparency document

The Transparency document associated with this article can be found, in online version.

Acknowledgments

The authors gratefully acknowledge financial support from EPSRC. Project: *Ionic Coulomb blockade oscillations and the physical origins of permeation, selectivity, and their mutation transformations in biological ion channels* (EPSRC reference: EP/M015831/1 and EP/M016889/1). Computational facilities were provided by the MidPlus Regional Centre of Excellence for Computational Science, Engineering and Mathematics, under EPSRC grant EP/K000128/1, and by the University of Warwick Scientific Computing Research Technology Platform. We are thankful to Dr Sun Huaping for her help in the generation of NaChBac mutant cDNA.

Appendix A. Supplementary data

Supplementary data to this article can be found online at https://doi.org/10.1016/j.bbamem.2018.11.011.

References

[1] D.J. Aidley, P.R. Stanfield, Ion Channels: Molecules in Action, Cambridge University Press, Cambridge UK, 1996.
[2] F.M. Ashcroft, Ion Channels and Disease, Academic Press, San Diego, USA, 1999.
[3] F. Bezanilla, C.F. Armstrong, Negative conductance caused by entry of sodium and cesium ions into the potassium channels of squid axons, J. Gen. Physiol. 60 (1972) 588–608.
[4] S.Y. Noskov, S. Berneche, B. Roux, Control of ion selectivity in potassium channels by electrostatic and dynamic properties of carbonyl ligands, Nature 431 (2004) 830–834.
[5] H. Yu, S.Y. Noskov, B. Roux, Two mechanisms of ion selectivity in protein binding sites, Proc. Natl. Acad. Sci. U. S. A. 107 (47) (2010) 20329–20334.

[6] J. Payandeh, T. Scheuer, N. Zheng, W.A. Catterall, The crystal structure of a voltage-gated sodium channel, Nature 475 (2011) 353–358.
[7] S. Furini, C. Domene, On conduction in a bacterial sodium channel, PLoS Comput. Biol. 8 (4) (2012) e1002476.
[8] B. Corry, M. Thomas, Mechanism of ion permeation and selectivity in a voltage gated sodium channel, J. Am. Chem. Soc. 134 (2012) 1840–1846.
[9] I.K. Kaufman, P.V.E. McClintock, R.S. Eisenberg, Coulomb blockade model of permeation and selectivity in biological ion channels, New J. Phys. 17 (2015).
[10] D. Ren, B. Navarro, H. Xu, L. Yue, Q. Shi, D.E. Clapham, A prokaryotic voltage-gated sodium channel, Science 294 (5550) (2001) 2372–2375.
[11] L. Yue, B. Navarro, D. Ren, A. Ramos, D.E. Clapham, The cation selectivity filter of the bacterial sodium channel, NaChBac, J. Gen. Physiol. 120 (2002) 845–853.
[12] W.A. Catterall, N. Zheng, Deciphering voltage-gated Na(+) and Ca(2+) channels by studying prokaryotic ancestors, Trends Biochem. Sci. 40 (9) (2015) 526–534.
[13] E.C. McCusker, C. Bagneris, C.E. Naylor, A.R. Cole, N. D'Avanzo, C.G. Nichols, B.A. Wallace, Structure of a bacterial voltage-gated sodium channel pore reveals mechanisms of opening and closing, Nat. Commun. 3 (2012) 1102.
[14] D. Shaya, F. Findeisen, F. Abderemane-Ali, C. Arrigoni, S. Wong, S.R. Nurva, G. Loussouarn, D.L. Minor, Structure of a prokaryotic sodium channel pore reveals essential gating elements and an outer ion binding site common to eukaryotic channels, J. Mol. Biol. 426 (2) (2014) 467–483.
[15] L. Tang, T.M. Gamal El-Din, J. Payandeh, G.Q. Martinez, T.M. Heard, T. Scheuer, N. Zheng, W.A. Catterall, Structural basis for Ca2+ selectivity of a voltage-gated calcium channel, Nature 505 (7481) (2014) 56–61.
[16] I.K. Kaufman, D.G. Luchinsky, R. Tindjong, P.V.E. McClintock, Energetics of discrete selectivity bands and mutation-induced transitions in the calcium-sodium ion channels family, Phys. Rev. E 88 (5) (2013) 052712.
[17] C. Guardiani, P.M. Rodger, O.A. Fedorenko, S.K. Roberts, I.A. Khovanov, Sodium Binding Sites and Permeation Mechanism in the NaChBac channel: a molecular dynamics study, J. Comput. Chem. 13 (2017) 1389–1400.
[18] C. Guardiani, O.A. Fedorenko, S.K. Roberts, I.A. Khovanov, On the selectivity of the NaChBac channel: an integrated computational and experimental analysis of sodium and calcium permeation, Phys. Chem. Chem. Phys. 19 (2017) 29840–29854.
[19] S. Jo, T. Kim, V.G. Iyer, W. Im, CHARMM-GUI: a web-based graphical user interface for CHARMM, J. Comput. Chem. 29 (2008) 1859–1865.
[20] E.L. Wu, X. Cheng, S. Jo, H. Rui, K.C. Song, E.M. Davila-Contreras, Y. Qi, J. Lee, V. Monje-Galvan, R.M. Venable, J.B. Klauda, W. Im, CHARMM-GUI Membrane builder toward realistic biological membrane simulations, J. Comput. Chem. 35 (2014) 1997–2004.
[21] J.C. Phillips, R. Braun, W. Wang, J. Gumbart, E. Tajkhorshid, E. Villa, C. Chipot, R.D. Skeel, L. Kale, K. Schulten, Scalable molecular dynamics with NAMD, J. Comput. Chem. 26 (2005) 1781–1802.
[22] J.A. Maier, C. Martinez, K. Kasavajhala, L. Wickstrom, K.E. Hauser, C. Simmerling, Ff14SB: improving the accuracy of protein side chain and backbone parameters from ff99SB, J. Chem. Theory Comput. 11 (2015) 3696–3713.
[23] C.J. Dickson, B.D. Madej, A.A. Skjevik, R.M. Betz, K. Teigen, I.R. Gould, R.C. Walker, Lipid14: the amber lipid force field, J. Chem. Theory Comput. 10 (2014) 865–879.
[24] M.B. Ulmschneider, C. Bagneris, E.C. McCusker, P.G. DeCaen, M. Delling, D.E. Clapham, J.P. Ulmschneider, B.A. Wallace, Molecular dynamics of ion transport through the open conformation of a bacterial voltage-gated sodium channel, Proc. Natl. Acad. Sci. U. S. A. 110 (16) (2013) 6364–6369.
[25] T.X. Dang, E.W. McCleskey, Ion channel selectivity through stepwise changes in binding affinity, J. Gen. Physiol. 111 (1998) 185–193.
[26] K.V. Lopin, C.A. Obejero-Paz, S.W. Jones, K.V. Lopin, C.A. Obejero-Paz, S.W. Jones, Evaluation of a two-site, three-barrier model for permeation in $Ca_v3.1$ (α1G) T-type calcium channels: Ca^{2+}, Ba^{2+}, Mg^{2+} and Na^{+}, J. Membr. Biol. 235 (2010) 131–143.
[27] N. Khan, I.P. Gray, C.A. Obejero-Paz, S.W. Jones, Permeation and gating in Cav3.1 (α1G) T-type calcium channels effects of Ca^{2+}, Ba^{2+}, Mg^{2+} and Na^{+}, J. Gen. Physiol. 132 (2008) 223–238.
[28] J. Wang, M. Kwiatkowski, M.Y. Pavlov, M. Ehrenberg, A.C. Forster, Peptide formation by N-methyl amino acids in translation is hastened by higher pH and $tRNA^{Pro}$, ACS Chem. Biol. 9 (2014) 1303–1311.
[29] T. Kawakami, H. Murukami, H. Suga, Messenger RNA-programmed incorporation of multiple N-methyl-amino acids into linear and cyclic peptides, Chem. Biol. 15 (2008) 32–42.
[30] A.O. Subtelny, M.C.T. Hartman, J.W. Szostak, Optimal codon choice can improve the efficiency and fidelity of n-methyl amino acid incorporation into peptides by in-vitro translation, Angew. Chem. Int. Ed. 50 (2011) 3164–3167.
[31] O.A. Fedorenko, I.K. Kaufman, W.A.T. Gibby, D.G. Luchinsky, S.K. Roberts, P.V.E. McClintock, Ionic coulomb blockade and the determinants of selectivity in the nachbac bacterial sodium channel, Biophys. J. (2018) Submitted for publication.
[32] E. Neher, Correction for liquid junction potentials in patch clamp experiments, Methods Enzymol. 207 (1992) 123–131.
[33] I. Kaufman, O.A. Fedorenko, D.G. Luchinsky, W.A.T. Gibby, S.K. Roberts, P.V.E. McClintock, R.S. Eisenberg, Ionic Coulomb blockade and anomalous mole fraction effect in the NaChBac bacterial ion channel and its charge-varied mutants, EPJ Nonlinear Biomed. Phys. 5 (8) (2017) 4.
[34] J. Yang, P.T. Ellinor, W.A. Sather, J.F. Zhang, R.W. Tsien, Molecular determinants of Ca^{2+} selectivity and ion permeation in L-type Ca^{2+} ion channels, Nature 366 (1993) 158–161.
[35] P.T. Ellinor, J. Yang, W.A. Sather, J.F. Zhang, R.W. Tsien, Ca^{2+} channel selectivity at a single locus for high-affinity Ca^{2+} interactions, Neuron 15 (1995) 1121–1132.
[36] S.H. Heinemann, H. Terlau, W. Stühmer, K. Imoto, S. Numa, Calcium channel characteristics conferred on the sodium channel by single mutations, Nature 356 (6368) (1992) 441–443.
[37] K. Talavera, M. Staes, A. Janssens, N. Klugbauer, G. Droogmans, F. Hofmann, B. Nilius, Aspartate residues of the Glu-Glu-Asp-Asp (EEDD) pore locus control selectivity and permeation of the T-type Ca^{2+} channel α_{1G}, J. Biol. Chem. 276 (2001) 45628–45635.
[38] K. Talavera, A. Janssens, N. Klugbauer, G. Droogmans, B. Nilius, K. Talavera, A. Janssens, N. Klugbauer, G. Droogmans, B. Nilius, Extracellular Ca^{2+} modulates the effects of protons on gating and conduction properties of the T-type Ca^{2+} channel α_{1G} ($Ca_v3.1$), J. Gen. Physiol. 121 (2003) 511–528.
[39] K. Talavera, A. Janssens, N. Klugbauer, G. Droogmans, B. Nilius, Pore structure influences gating properties of the T-type Ca^{2+} channel α_{1G}, J. Gen. Physiol. 121 (2003) 529–540.
[40] W. Im, B. Roux, Ion permeation and selectivity of OmpF porin: a theoretical study based on molecular dynamics, Brownian dynamics, and continuum electrodiffusion theory, J. Mol. Biol. 322 (2002) 851–869.